Controllable Atomic Scale Patterning of Freestanding Monolayer Graphene at Elevated Temperature

Qiang Xu,[†] Meng-Yue Wu,[†] Grégory F. Schneider,[†] Lothar Houben,[‡] Sairam K. Malladi,[†] Cees Dekker,[†] Emrah Yucelen,[§] Rafal E. Dunin-Borkowski,[‡] and Henny W. Zandbergen[†,*]

[†]Kavli Institute of Nanoscience, Delft University of Technology, Lorentzweg 1, 2628 CJ Delft, The Netherlands, [‡]Ernst Ruska-Centre for Microscopy and Spectroscopy with Electrons and Peter Grünberg Institute, Forschungszentrum Jülich, D-52425 Jülich, Germany, and [§]FEI Company, Europe NanoPort, Achtseweg Noord 5, 5651 GG Eindhoven, The Netherlands

ABSTRACT We show that by operating a scanning transmission electron microscope (STEM) with a 0.1 nm 300 kV electron beam, one can sculpt free-standing monolayer graphene with close-to-atomic precision at 600 °C. The same electron beam that is used for destructive sculpting can be used to image the sculpted monolayer graphene nondestructively. For imaging, a scanning dwell time is used that is about 1000 times shorter than for the sculpting. This approach allows for instantaneous switching between sculpting and imaging and thus fine-tuning the shape of the sculpted lattice. Furthermore, the sculpting process can be automated using a script. In this way, free-standing monolayer graphene can be controllably sculpted into patterns that are predefined in position, size, and orientation while maintaining defect-free crystallinity of the adjacent lattice. The sculpting and imaging processes can be fully computer-controlled to fabricate complex assemblies of ribbons or other shapes.

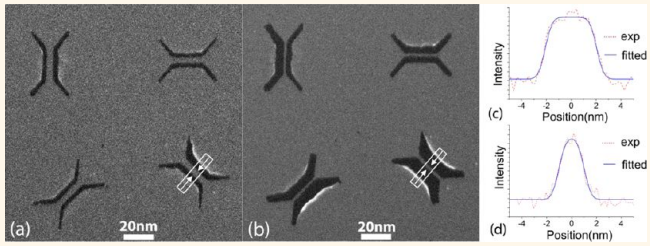

KEYWORDS: scanning transmission electron microscopy · graphene · controlled sculpting · nondestructive imaging · nanopatterning · self-repair

The rapidly increasing research effort into studies of graphene since 2004[1−5] has resulted from its superior mobility, strength, and thermal conductivity,[6−8] both for low-dimensional physics research and for applications such as field-effect transistors, photonic and optoelectronic devices, single-molecule detection, and fast DNA sequencing.[9−13] Many of these applications require monolayer graphene to be patterned into ribbons, gaps, or pores, whose edge configurations need to be defined with sub-nanometer precision.

As both theoretical and experimental studies have shown that the edges and geometries of graphene sheets can have a fundamental influence on their electronic and magnetic properties,[14−17] a controllable and reproducible atomic-scale technique for patterning monolayer graphene is required. For example, 2.5 nm wide nanoribbons with controlled armchair edge orientations have been predicted to open up the energy gap of graphene to 0.5 eV; zigzag nanoribbons are semiconducting with spin-polarized edges, and the band gaps of graphene ribbons are expected to be inversely proportional to their width.[18,19] Similarly, the size of nanopores needs to have a diameter of only 1−10 nm to control and monitor the translocation of a single-stranded DNA molecule. Ultimately, graphene engineering is intended to involve the artificial introduction and control of all defects in graphene at the atomic level. However, until now, no conclusive experimental verification has been obtained for the theoretical predictions of the physical properties of narrow graphene ribbons, primarily because it was impossible to make free-standing ribbons that are only a few nanometers wide, crystalline up to their edges, defect-free, and oriented in specific crystallographic directions in a controlled manner.

Several methods have been reported for patterning graphene.[20−23] Among these, scanning tunneling microscopy (STM) lithography[21] and focused electron beam etching in a transmission electron microscope

* Address correspondence to h.w.zandbergen@tudelft.nl.

Received for review November 19, 2012 and accepted January 23, 2013.

Published online January 23, 2013
10.1021/nn3053582

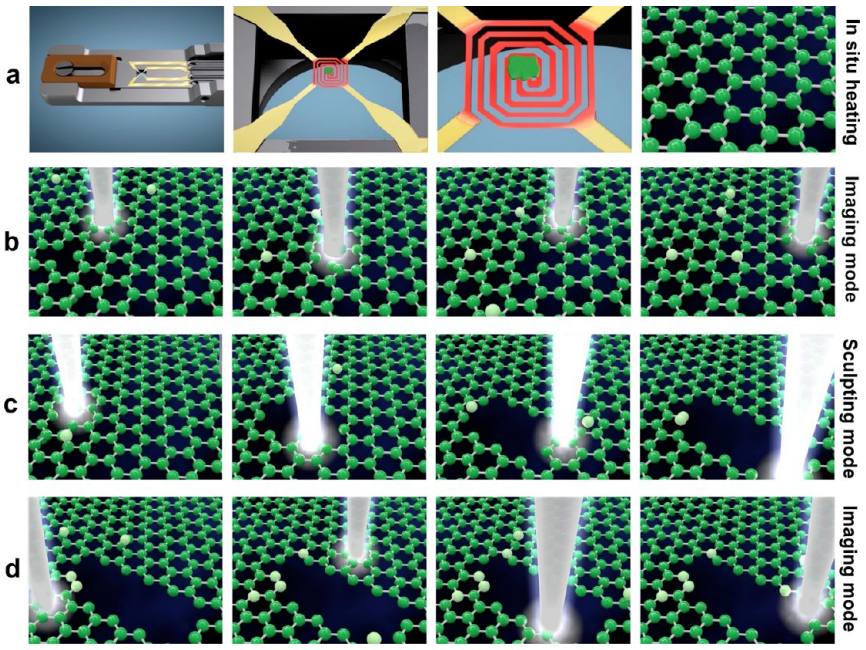

Figure 1. Schematic diagrams illustrating the experimental setup for sculpting graphene using STEM (frames taken from movie S1, Supporting Information). (a) MEMS heater used for ultrastable *in situ* heating of graphene inside the TEM. Heating is used for self-repair of graphene defects. (b) STEM imaging of graphene is achieved by fast scanning of the electron probe. A small number of C vacancies, created by the electron beam, can be efficiently self-repaired by the diffusion of C adatoms (lighter green spheres) over the graphene surface. (c) Sculpting is achieved by scanning exactly the same electron probe 1000 times slower by using a longer dwell time, which allows ensembles of defects to form stable voids. (d) Nondestructive imaging of the sculpted graphene can be achieved by switching back to the fast scan imaging mode.

(TEM)[23−26] have the potential to provide atomic-scale sculpting and orientation control, while also providing an imaging capability that allows validation of the sculpted pattern. We have previously shown that a TEM operated in high-resolution TEM (HRTEM) mode can be used to make nanobridges in free-standing *multilayer* graphene at elevated temperature.[23] However, the reproducible sculpting of a single ribbon or pore in either multilayer or monolayer graphene was impossible due to the uncontrolled formation of small holes in the neighborhood of the sculpted area.

In this paper, we report a reliable method to make monolayer graphene nanostructures. We show that scanning transmission electron microscopy (STEM)[27−29] in combination with *in situ* heating of the specimen to 500−700 °C allows reproducible patterning of free-standing monolayer graphene with close-to-atomic precision. STEM is essential to reduce the electron beam size and for accurate control of the electron irradiation dose at atomic level, while heating is essential for the active self-repair of any electron-beam-induced point defects created during the imaging process.

RESULTS AND DISCUSSION

Figure 1 and movie S1 in Supporting Information show schematic diagrams of the experimental setup. Sculpting of monolayer graphene was carried out at an elevated temperature of 500−700 °C using an ultrastable specimen heating holder based on a coiled Pt wire embedded in a SiN membrane[30] (Figure 1a). An FEI Titan G2 60-300 TEM was used in STEM mode, with an electron beam diameter of 0.1 nm and a beam current of 0.15 nA. In this mode, the electron dose can be controlled by using either the beam current or the dwell time (*i.e.*, the time for which the electron beam is kept at a given position). In practice, the dwell time is the most convenient parameter to use for adjusting the electron dose to select either destructive sculpting or nondestructive imaging. First, in imaging mode, a short dwell time (5−30 μs per pixel) was used at 600 °C to inspect the graphene and to select an area for sculpting. During imaging, any isolated defects (*i.e.*, vacancies) that are created by the electron beam are removed by self-repair of the lattice at elevated temperature (Figure 1b). Second, in sculpting mode, patterning is carried out by scanning the electron beam using a longer dwell time (>10 ms per pixel). At the beginning of this process, several adjacent C atoms are knocked out and the graphene lattice can no longer self-repair. By extending this initial hole in a predefined direction, the graphene can be shaped into a pattern that has a well-defined position, size, and orientation (Figure 1c). Third, by switching again to imaging mode, the sculpted pattern can be inspected without introducing further damage (Figure 1d). Details of the experimental parameters for achieving destructive sculpting and nondestructive imaging are described in Methods and Supporting Information.

Nanoribbons and nanopores are the most common shapes that have been proposed for graphene

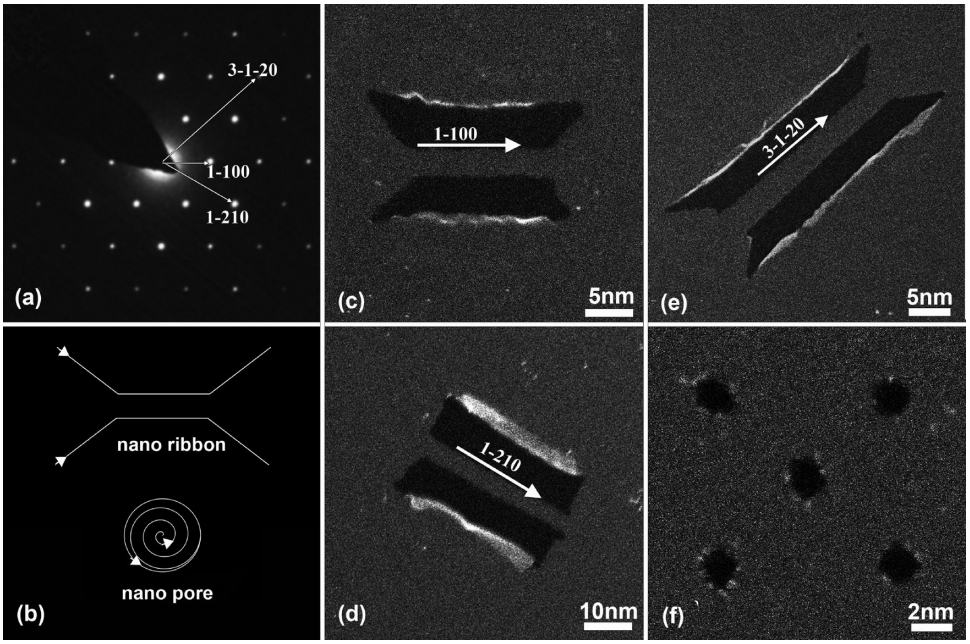

Figure 2. Examples of results of sculpting graphene using STEM. (a) Electron diffraction pattern revealing the crystal orientation and allowing verification that the graphene is a monolayer with the intensity ratio between (1$\bar{1}$00) and (1$\bar{2}$10) reflections larger than 1. (b) Paths (white lines) used to sculpt nanoribbons and nanopores. (c–f) Annular dark-field STEM images of (c–e) nanoribbons sculpted along ⟨1$\bar{1}$00⟩, ⟨1$\bar{2}$10⟩, and ⟨1$\bar{3}$20⟩ directions, respectively, and (f) an array of 2 nm diameter holes.

applications. Figure 2 shows examples of these shapes made using the present approach. We used diffraction patterns (Figure 2a) to monitor the orientation of the crystalline specimen in order to achieve crystal-lattice-related sculpting (*e.g.*, to specifically form zigzag edges). Electron diffraction patterns (the intensity ratio between 1$\bar{1}$00 and 1$\bar{2}$10 reflection should be larger than 1 for monolayers) and Raman spectra (see Supporting Information) were used to verify that the graphene is monolayered.[3] Nanoribbons were formed by moving the electron beam along two lines, while nanopores are formed by scanning the electron beam in a spiral manner starting from the center (Figure 2b). Figure 2c–d shows dark-field STEM images of nanoribbons that have been patterned along ⟨1$\bar{1}$00⟩, ⟨1$\bar{2}$10⟩, and ⟨1$\bar{3}$20⟩ crystallographic directions, corresponding to armchair, zigzag, and mixed edge configurations, respectively. Figure 2f shows a sculpted array of five 2 nm diameter holes, which demonstrate the reproducibility of the sculpted pattern that can be achieved, for instance, to create an antidot lattice.[31] The STEM image of the five pores shows ~0.5 nm patches of double-layer graphene close to the edges of some of the holes, suggesting that C atoms or graphene fragments that were removed during sculpting can remain attached in their close vicinity as clusters of adatoms. As the distance between adjacent spiral lines was 0.5–1.2 nm, some of the graphene located between the cutting lines may have remained on the edges of the holes. Similar single holes in graphene, ranging from 5 to 20 nm in diameter, have been used for DNA translocation and ionic transport measurements[12] without showing any degradation during storage in air or water for one month.

High-resolution TEM images of nanoribbons that had been sculpted at 300 kV along ⟨1$\bar{1}$00⟩, ⟨1$\bar{2}$10⟩, and ⟨1$\bar{3}$20⟩ crystallographic directions were made at 80 kV instead of 300 kV to reduce knock-out damage and at a temperature 600 °C to activate self-repair, using an FEI PICO TEM equipped with a combined spherical and chromatic objective lens aberration corrector (Figure 3). Atomically straight edges are visible in the ⟨1$\bar{1}$00⟩ (zigzag) and ⟨1$\bar{2}$10⟩ (armchair) directions. In other directions, the edges are usually made up of zigzag and armchair fragments, suggesting that these are the most stable configurations. Occasional regions where the edges of the zigzag and armchair fragments are not atomically straight (varying over a distance of one hexagonal C ring) may have resulted from slight instabilities in the positioning of the electron beam. Interestingly, on heating to ~800 °C, we observed that a curved edge of a hole in graphene became reconstructed into several straight armchair edges (see Figure S4 in Supporting Information), suggesting that further heat treatment can be used to improve the sharpness of armchair edges.

For all of the ribbons, the HRTEM images (Figure 3) show that the graphene lattice has remained defect-free and crystalline up to its edge, confirming that STEM imaging using 300 kV electrons in fast scanning mode at elevated temperature does not lead to damage that cannot be annihilated by self-repair. During

TEM imaging at 80 kV/600 °C, non-zigzag or non-armchair edges tend to restructure to form zigzag and armchair edges, but the zigzag and armchair edges are overall stable, in contrast with literature. In fact, we only observed damage when small agglomerates were present, which might contain metal atoms. The damage to the graphene is thus not by electron knock-out damage but by an electron-beam-stimulated metal-catalyzed reaction (see Figure S7 of Supporting Information).[32] Our results indicate that knock-out of C atoms at zigzag and armchair edges can be repaired as easily by self-repair as the graphene lattice itself. Likewise, we did not observe within the unsculpted/pristine graphene parts any type of Stone–Wales transformations, which are reported as being easy to observe at room temperature under a 80 kV electron beam, indicating that such defects are not formed or repaired quickly at high temperature. Also, the geometry and dynamics of the edges at high temperatures are temperature-sensitive (see Supporting Information).

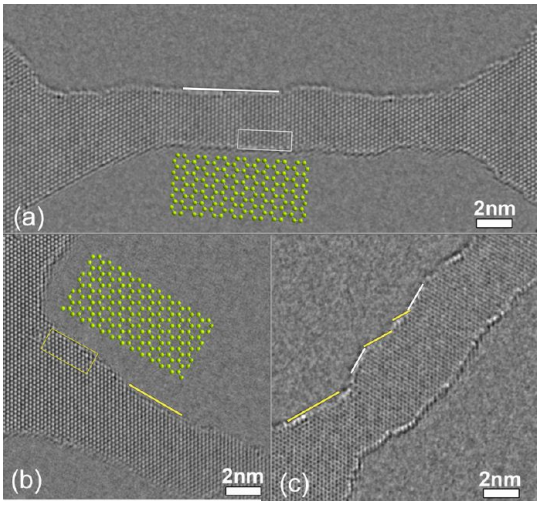

Figure 3. (a–c) HRTEM images of nanoribbons in monolayer graphene sculpted at 300 kV at 600 °C and imaged at 80 kV at 600 °C for ribbons oriented along ⟨1$\bar{1}$00⟩, ⟨1$\bar{2}$10⟩, and ⟨1$\bar{3}$20⟩, respectively. The overlaid white and yellow lines indicate armchair and zigzag edges, respectively. Atom structure models for armchair and zigzag edges, outlined with open frames in the corresponding images, are enlarged and overlaid.

Nondestructive imaging, which is possible in fast scanning STEM mode, provides the advantage that the sculpted pattern can be checked immediately using the same electron beam that was used for sculpting, that is, without compromising the stability of the specimen or the electron probe. Furthermore, based on the feedback provided by imaging, the shape of the pattern can be fine-tuned. An example of such fine-tuning is shown in Figure 4, illustrating the precision of the sculpting process. First, four nanoribbon patterns were sculpted and imaged (Figure 4a). On the basis of the geometry of the ribbons and taking sample drift into account, a second sculpting process was then applied to all four ribbons to achieve final widths of ~1.9 nm, that is, a width of only ~8 benzene rings (Figure 4d), demonstrating that reproducible sculpting with close-to-atomic precision is possible. This is evidently different from previous electron beam etching studies,[23,24] in which only a single nanoribbon was produced. Script-controlled sculpting promises to further improve the accuracy and reproducibility of such sculpting. By increasing the electron beam current to 5 nA, we achieved sculpting of a nanoribbon in 1 s, suggesting that large-scale patterning of graphene may also be possible.

The preservation of a defect-free graphene lattice following STEM imaging is a direct consequence of the self-repair of electron-beam-induced point defects at elevated temperature. The effect of specimen temperature was investigated by performing sculpting at 20, 400, 600, 700, and 800 °C under identical STEM conditions using various dwell times. For most monolayer graphene flakes, attempts at sculpting resulted only in contamination at 20 °C, whereas sculpting

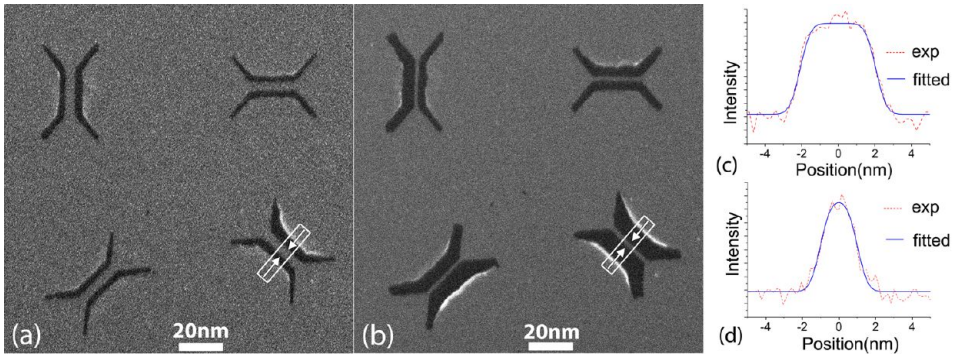

Figure 4. (a,b) Annular dark-field STEM images of a nanoribbon array, illustrating the reproducibility of the sculpting. The four patterns were created using a script-controlled electron beam. After the first sculpting process, the patterns were imaged as shown in (a). Next, each ribbon was reduced in width precisely, and image (b) was acquired. Intensity line profiles across the ribbon outlined by the white frames in (a) and (b) are shown in (c) and (d), respectively. The width of the ribbon is estimated to be 4.0 ± 0.1 nm after initial sculpting and 1.9 ± 0.1 nm after final sculpting, by fitting the experimental profiles with top-hat functions convoluted with Gaussians to take beam spread into account.

could be performed easily at 400, 600, and 700 °C. At 800 °C, sculpting was again not possible, even if very long dwell times were used, indicating that self-repair is faster than carbon removal. Interestingly, when examining a "super clean" graphene sample, sculpting was possible at all of the investigated temperatures with roughly the same speed. STEM imaging of super clean graphene at 600 °C resulted in no visible (extended) defects. These observations indicate that both temperature and the cleanliness of the specimen play a key role in the sculpting process. If the specimen is "dirty", then at elevated temperature, self-repair takes place instead of sculpting, while at lower temperature, contamination takes place instead of sculpting. We tried to repeat the preparation of super clean graphene samples and managed only twice out of 300 trials; we have not found how this can be done reproducibly.

Our results suggest that the sculpting of graphene using a high-energy electron beam involves three primary processes: (1) the formation of vacancies by knock-on damage; (2) self-repair of the graphene lattice by C adatoms or C-rich ad-molecules; (3) the electron-beam-induced formation of C-rich contamination due to the cracking of hydrocarbons diffusing over the surface toward the electron beam. The second and third of these processes are highly temperature-dependent. The results of imaging super clean graphene show that, even in this case, there are enough C adatoms on the surface for self-repair at 600 °C and that the buildup of C contamination on dirty graphene below 300 °C does not result from the presence of the C adatoms but from cracking of hydrocarbons (originating mainly from the sample and the sample holder). In our experiments, *in situ* heating above ~300 °C was found to prevent the buildup of contamination on all of the graphene samples.

Knock-on damage results when a high-energy incident electron hits the core of a C atom and knocks the atom out of lattice, whereby the electron itself is backscattered. Due to the very small mass of an electron compared to that of a C atom, the chance of knock-on damage is very small. For 300 kV electrons, the cross section for C knock-on damage (the target size of the core) is ~10 barn.[33,34] For a 0.1 nm probe, the size of electron beam is $\sim 10^8$ barn. Thus, the possibility of knocking one carbon atom out by the 0.1 nm e-beam probe is $\sim 10^{-7}$, or in other words, $\sim 10^7$ electrons are required to achieve one C knock-on damage event. An electron beam with a current of 0.15 nA and a dwell time of ~10 ms provides this number of electrons and should thus, on average, be able to create one C vacancy. This estimate is consistent with our observations for sculpting. In contrast, fast scan imaging performed using a 10 μs dwell time results in a radiation dose of approximately 10^4 electrons/atom and thus only a 10^{-3} probability of creating a C vacancy. Therefore, when fast scanning a 512 × 512 pixel STEM image, on average, ~260 vacancies are generated since e-beam is positioned on ~260 000 pixels (512^2), and these vacancies are annihilated by self-repair at elevated temperature before they cluster to form larger, more stable defects.

Self-repair requires either C diffusion over the graphene surface toward a vacancy or vacancy migration. As the C adatom surface diffusion energy has been reported to be 0.2−0.5 eV[35] and the energy for vacancy diffusion is ~1.2 eV,[35] repair by the diffusion of C adatoms (if they are present) is expected to dominate. Sources of C adatoms may include adsorbed hydrocarbons, C atoms remaining from exfoliation, and C atoms knocked out by the electron beam. Increasing the temperature accelerates the diffusion speed of surface C adatoms such that electron-beam-induced vacancies are annihilated more actively.

Dark-field STEM imaging provides better contrast to identify the edge of a pattern and to achieve automated control of sculpting than bright-field HREM imaging (see Figures 3 and 4 and the Supporting Information). In our dark-field STEM images, electrons scattered to angles between 10 and 60 mrad were collected. The cross section for scattering a 300 kV electron into this angular range is $\sim 3.5 \times 10^5$ barn, that is, 4 orders of magnitude greater than that for knock-on damage. Therefore, when using a short dwell time for STEM imaging to reduce knock-on damage, one can still collect a sufficient number of electrons to form a good image. Optimization of image contrast in relation to sculpting speed can be achieved by changing the accelerating voltage, as discussed in the Supporting Information.

The next step will be to fabricate a complete device, allowing electrical measurements combined with *in situ* TEM. This requires the following steps: (1) mounting of a small graphene flake on electrodes, (2) making a nanoribbon, (3) removing the remaining part of the graphene to allow passing a current only through the nanoribbon, (4) performing electrical measurements in which we could add some additional sculpting. For step 1, one has to mount a piece of graphene onto the electrodes with a precision of several micrometers; it is well possible to do this with the wedging transfer method used in this paper and described in detail elsewhere.[36] Step 2 is possible by STEM sculpting as described in this paper. Step 3 is expected to be doable with STEM (but time-consuming) or, alternatively, with a helium ion beam. The main challenge will be to minimize the strain sufficiently, such that the nanoribbon does not break or change significantly. Step 4 requires very sensitive electronics, such as the one we described earlier in a paper on *in situ* TEM analysis of current-induced grain growth.[37]

CONCLUSIONS

In conclusion, it is possible to reproducibly sculpt monolayer graphene with close-to-atomic precision using a 300 kV 0.1 nm diameter focused electron beam if an elevated specimen temperature is used to achieve self-repair. Significantly, the sculpted pattern can be imaged nondestructively using the same microscope settings and a dwell time that is ~1000 times shorter in STEM. The sculpting and imaging processes can be fully computer-controlled to fabricate complex assemblies of ribbons or other shapes. The use of a high-brightness electron source allows a device with, for instance, 10 bridges to be made within a minute. This is too slow for large-scale production but certainly good enough for making prototypes of graphene devices. The resulting patterned structures are stable upon cooling the graphene to room temperature and storing it in air. This method opens the possibility to accurately pattern free-standing graphene and other graphene-like materials.

METHODS

Sample Preparation and Transfer. Graphene flakes were prepared by the exfoliation of natural graphite (NGS graphite) onto a 285 nm thermally grown SiO_2/Si wafer. Graphene flakes of interest were selected using optical interference microscopy and transferred over a hole on a SiN membrane using a "wedging" transfer technique.[36] The crystallinity and single-layer nature of each graphene flake were confirmed using electron diffraction and Raman spectroscopy (see Supporting Information).

Heating Holder with MEMS Heater for *In Situ* Experiments. We used an *in situ* single tilt TEM heating holder (DENSsolutions: SH30), in which a SiN membrane containing an embedded coiled Pt wire[30] was used for substrate-free *in situ* heating of graphene flakes, which were each placed over a 2 μm diameter hole made through both the SiN membrane and the Pt heating wire using a focused Ga ion beam. The low heat capacity of the system results in very low thermal drift (less than 0.1 nm/min) at elevated temperature, which is essential for accurate STEM sculpting, as specimen drift greatly influences the deviation between a predefined pattern and a final sculpted result. No significant change in the vacuum of the TEM was observed upon switching on the heater, which is consistent with the small surface area of the heated region (0.3 × 0.3 mm).

Parameters for STEM Sculpting and Imaging. STEM imaging of nanopatterned graphene was performed at 300 kV using an FEI Titan^3 G2 60-300 TEM equipped with a postspecimen spherical aberration (C_S) corrector. The electron beam convergence semiangle was chosen to be 10 mrad to achieve the smallest incident focused electron beam (0.12−0.14 nm diameter). The camera length was set to 470 mm to allow the annular detector to record the maximum number of diffracted electron beams from graphene, in an angular range of 10−60 mrad. The electron beam current was set to 0.15 nA (acquired using the microscope software) for STEM imaging and sculpting. The dwell time was chosen to be 5−30 μs for imaging and 10−80 ms for sculpting.

Parameters for High-Resolution TEM Imaging at 80 kV. High-resolution TEM images were recorded at 80 kV with the sample at 600 °C using an FEI Titan 60-300 PICO TEM equipped with a high-brightness electron gun, an electron gun monochromator, a probe aberration corrector, and a C_S−C_C image corrector. Typical exposure times were 2 s. Image series were acquired for averaging; typically, about 10 images were acquired using a 2 s acquisition time onto a 4 k × Gatan charge-coupled device (CCD) camera set to 2 × 2 binning. The image sequences were aligned and averaged using ImageJ software.[38]

Conflict of Interest: The authors declare no competing financial interest.

Acknowledgment. This work is financially supported by FOM-program 08IP05 in The Netherlands. The authors dedicate this article to Prof. Jing Zhu, for her 75th birthday and 50 years of serving her motherland.

Supporting Information Available: Raman spectroscopy of monolayer graphene; discussion of control parameters for destructive STEM sculpting and nondestructive imaging; edge reconstruction at 800 °C; comparison of sculpting at room temperature, 600, and 800 °C; agglomerates on graphene and their effect on hole formation; optimization of electron beam energy for imaging and sculpting, contrast comparison in STEM and HRTEM; animation movies of *in situ* controllable STEM sculpting free-standing graphene and self-repair at 800 °C. This material is available free of charge *via* the Internet at http://pubs.acs.org.

REFERENCES AND NOTES

1. Novoselov, K. S.; Geim, A. K.; Morozov, S. V.; Jiang, D.; Zhang, Y.; Dubonos, S. V.; Grigorieva, I. V.; Firsov, A. A. Electric Field Effect in Atomically Thin Carbon Films. *Science* **2004**, *306*, 666–669.
2. Zhang, Y.; Tan, Y.-W.; Stormer, H. L.; Kim, P. Experimental Observation of the Quantum Hall Effect and Berry's Phase in Graphene. *Nature* **2005**, *438*, 201–204.
3. Meyer, J. C.; Geim, A. K.; Katsnelson, M. I.; Novoselov, K. S.; Booth, T. J.; Roth, S. The Structure of Suspended Graphene Sheets. *Nature* **2007**, *446*, 60–63.
4. Geim, A. K.; Novoselov, K. S. The Rise of Graphene. *Nat. Mater.* **2007**, *6*, 183–191.
5. Geim, A. K.; Kim, P. Carbon Wonderland. *Sci. Am.* **2008**, *298*, 90–97.
6. Castro Neto, A. H.; Guinea, F.; Peres, N. M. R.; Novoselov, K. S.; Geim, A. K. The Electronic Properties of Graphene. *Rev. Mod. Phys.* **2009**, *81*, 109–162.
7. Lee, C.; Wei, X.; Kysar, J. W.; Hone, J. Measurement of the Elastic Properties and Intrinsic Strength of Monolayer Graphene. *Science* **2008**, *321*, 385–388.
8. Girit, Ç. Ö.; Meyer, J. C.; Erni, R.; Rossell, M. D.; Kisielowski, C.; Yang, L.; Park, C.-H.; Crommie, M. F.; Cohen, M. L.; Louie, S. G.; *et al.* Graphene at the Edge: Stability and Dynamics. *Science* **2009**, *323*, 1705–1708.
9. Li, X.; Wang, X.; Zhang, L.; Lee, S.; Dai, H. Chemically Derived, Ultrasmooth Graphene Nanoribbon Semiconductors. *Science* **2008**, *319*, 1229–1232.
10. Schwierz, F. Graphene Transistors. *Nat. Nanotechnol.* **2010**, *5*, 487–496.
11. Min, S. K.; Kim, W. Y.; Cho, Y.; Kim, K. S. Fast DNA Sequencing with a Graphene-Based Nanochannel Device. *Nat. Nanotechnol.* **2011**, *6*, 162–165.
12. Schneider, G. F.; Kowalczyk, S. W.; Calado, V. E.; Pandraud, G.; Zandbergen, H. W.; Vandersypen, L. M. K.; Dekker, C. DNA Translocation through Graphene Nanopores. *Nano Lett.* **2010**, *10*, 3163–3167.
13. Garaj, S.; Hubbard, W.; Reina, A.; Kong, J.; Branton, D.; Golovchenko, J. A. Graphene as a Subnanometre trans-Electrode Membrane. *Nature* **2010**, *467*, 190–193.
14. Han, M. Y.; Özyilmaz, B.; Zhang, Y.; Kim, P. Energy Band-Gap Engineering of Graphene Nanoribbons. *Phys. Rev. Lett.* **2007**, *98*, 206805–206805.
15. Son, Y.-W.; Cohen, M. L.; Louie, S. G. Half-Metallic Graphene Nanoribbons. *Nature* **2006**, *444*, 347–349.
16. Ribeiro, R.; Poumirol, J.-M.; Cresti, A.; Escoffier, W.; Goiran, M.; Broto, J.-M.; Roche, S.; Raquet, B. Unveiling the

Magnetic Structure of Graphene Nanoribbons. *Phys. Rev. Lett.* **2011**, *107*, 086601–086601.
17. Han, M. Y.; Brant, J. C.; Kim, P. Electron Transport in Disordered Graphene Nanoribbons. *Phys. Rev. Lett.* **2010**, *104*, 056801–056801.
18. Son, Y.-W.; Cohen, M. L.; Louie, S. G. Energy Gaps in Graphene Nanoribbons. *Phys. Rev. Lett.* **2006**, *97*, 216803.
19. Jung, J.; Pereg-Barnea, T.; MacDonald, A. H. Theory of Interedge Superexchange in Zigzag Edge Magnetism. *Phys. Rev. Lett.* **2009**, *102*, 227205.
20. Kato, T.; Hatakeyama, R. Site- and Alignment-Controlled Growth of Graphene Nanoribbons from Nickel Nanobars. *Nat. Nanotechnol.* **2012**, *7*, 651–656.
21. Tapaszto, L.; Dobrik, G.; Lambin, P.; Biro, L. P. Tailoring the Atomic Structure of Graphene Nanoribbons by Scanning Tunnelling Microscope Lithography. *Nat. Nanotechnol.* **2008**, *3*, 397–401.
22. Wang, X.; Dai, H. Etching and Narrowing of Graphene from the Edges. *Nat. Chem.* **2010**, *2*, 661–665.
23. Song, B.; Schneider, G. F.; Xu, Q.; Pandraud, G.; Dekker, C.; Zandbergen, H. Atomic-Scale Electron-Beam Sculpting of Near-Defect-Free Graphene Nanostructures. *Nano Lett.* **2011**, *11*, 2247–2250.
24. Jin, C.; Lan, H.; Peng, L.; Suenaga, K.; Iijima, S. Deriving Carbon Atomic Chains from Graphene. *Phys. Rev. Lett.* **2009**, *102*, 205501.
25. Zobelli, A.; Gloter, A.; Ewels, C. P.; Colliex, C. Shaping Single Walled Nanotubes with an Electron Beam. *Phys. Rev. B* **2008**, *77*, 045410.
26. Yuzvinsky, T. D.; Mickelson, W.; Aloni, S.; Begtrup, G. E.; Kis, A.; Zettl, A. Shrinking a Carbon Nanotube. *Nano Lett.* **2006**, *6*, 2718–2722.
27. Browning, N. D.; Chisholm, M. F.; Pennycook, S. J. Atomic-Resolution Chemical Analysis Using a Scanning Transmission Electron Microscope. *Nature* **2006**, *444*, 235–235.
28. Batson, P. E.; Dellby, N.; Krivanek, O. L. Corrigendum: Sub-angstrom Resolution Using Aberration Corrected Electron Optics. *Nature* **2002**, *419*, 94–94.
29. Huang, P. Y.; Ruiz-Vargas, C. S.; van der Zande, A. M.; Whitney, W. S.; Levendorf, M. P.; Kevek, J. W.; Garg, S.; Alden, J. S.; Hustedt, C. J.; Zhu, Y.; *et al.* Grains and Grain Boundaries in Single-Layer Graphene Atomic Patchwork Quilts. *Nature* **2011**, *469*, 389–392.
30. van Huis, M. A.; Young, N. P.; Pandraud, G.; Creemer, J. F.; Vanmaekelbergh, D.; Kirkland, A. I.; Zandbergen, H. W. Atomic Imaging of Phase Transitions and Morphology Transformations in Nanocrystals. *Adv. Mater.* **2009**, *21*, 4992–4995.
31. Pedersen, T. G.; Flindt, C.; Pedersen, J.; Mortensen, N. A.; Jauho, A.-P.; Pedersen, K. Graphene Antidot Lattices: Designed Defects and Spin Qubits. *Phys. Rev. Lett.* **2008**, *100*, 136804.
32. Zan, R.; Bangert, U.; Ramasse, Q.; Novoselov, K. S. Interaction of Metals with Suspended Graphene Observed by Transmission Electron Microscopy. *J. Phys. Chem. Lett.* **2012**, *3*, 953–958.
33. Egerton, R. F.; McLeod, R.; Wang, F.; Malac, M. Basic Questions Related to Electron-Induced Sputtering in the TEM. *Ultramicroscopy* **2010**, *110*, 991–997.
34. Zobelli, A.; Gloter, A.; Ewels, C. P.; Seifert, G.; Colliex, C. Electron Knock-on Cross Section of Carbon and Boron Nitride Nanotubes. *Phys. Rev. B* **2007**, *75*, 245402–245402.
35. Banhart, F.; Kotakoski, J.; Krasheninnikov, A. V. Structural Defects in Graphene. *ACS Nano* **2010**, *5*, 26–41.
36. Schneider, G. F.; Calado, V. E.; Zandbergen, H.; Vandersypen, L. M. K.; Dekker, C. Wedging Transfer of Nanostructures. *Nano Lett.* **2010**, *10*, 1912–1916.
37. Gao, B.; Rudneva, M.; McGarrity, K. S.; Xu, Q.; Prins, F.; Thijssen, J. M.; Zandbergen, H.; van der Zant, H. S. J. *In Situ* Transmission Electron Microscopy Imaging of Grain Growth in a Platinum Nanobridge Induced by Electric Current Annealing. *Nanotechnology* **2011**, *22*, 205705.
38. Rasband, W. S. *ImageJ*, 1.45; National Institute of Mental Health: Bethesda, MD, 2011.